



Sunlight mediated photocatalytic degradation of organic pollutants by statistical optimization of green synthesized NiO NPs as catalyst

Selvaraj Mohana Roopan^{a,*}, Ganesh Elango^{a,b,1}, D. Devi Priya^{a,1}, I.V. Asharani^c, Basker Kishore^a, Sharma Vinayprabhakar^a, Narayanan Pragatheshwaran^a, Kalisamy Mohanraj^a, Rajan Harshpriya^a, Shajahan Shanavas^{d,e}, Roberto Acevedo^e

^a Chemistry of Heterocycles and Natural Product Research Laboratory, Department of Chemistry, School of Advanced Science, Vellore Institute of Technology, Vellore, Tamilnadu 632014, India

^b Department of Biotechnology, Jaya College of Arts and Science, Thiruninravur, Chennai, Tamil Nadu 602024, India

^c Department of Chemistry, School of Advanced Science, Vellore Institute of Technology, Vellore, Tamilnadu 632 014, India

^d Nano and Hybrid Materials Laboratory, Department of Physics, Periyar University, Salem, Tamil Nadu 636 011, India

^e Facultad de Ingeniería y Tecnología, Universidad San Sebastián, Bellavista 7, Santiago 8420524, Chile

ARTICLE INFO

Article history:

Received 26 February 2019

Received in revised form 24 July 2019

Accepted 4 August 2019

Available online 05 August 2019

Keywords:

C. gigantea

Latex

NiO NPs

Azo dye

Nitrophenol

Kinetics

ABSTRACT

In this manuscript we have prepared nickel oxide nanoparticles (NiO NPs) using *Calotropis gigantea* latex (CGL) through green synthesis method in which the latex acts as a capping agent. The synthesis part was optimized using RSM-BBD methodology. Further the synthesized NiO NPs were subjected to various analytical techniques like UV–Visible spectroscopy, Transmission Electron Microscope (TEM), X-ray diffractometer (XRD), Energy Dispersive Analysis (EDX), Particle Size Histogram and Zeta potential. We observed the cuboidal shape of NiO NPs with 28 ± 2 nm as average particle size. Further the synthesized NiO NPs were subjected to degrade toxic diazo dye Congo red (CR) and organic compound 4-Nitro phenol in the presence of sunlight within short duration of time. The results indicate that the NiO NPs degrades 95% of CR and 94% of nitro phenol.

© 2019 Elsevier B.V. All rights reserved.

1. Introduction

Development of nanotechnology and nanoscience is limitless in the current century [1,2]. When contrasting with other metals, nanoparticles of transition metals have a favourable potency, so for synthesis of transition metal nanoparticles are preferred [3,4]. The application of the synthesized nanoparticles varies depending upon the shape, size, surface morphology, structure and composition [5–7]. Nanoparticles possess unique optical, magnetic, electronic and chemical properties [5,7–9]. Nanoparticles helps in developing the advanced chemical sensors, electronic devices etc. There are 3 fundamental practices for nanoparticles synthesise such as chemical, biological, and chemical approaches. Chemical and physical methods will require more investment and consume more time which likely results in toxic final product. Henceforth the non-poisonous and least expensive natural (biological) methodology was picked for nanoparticles synthesis [10–12]. Comparing to other methods, biological approach was ecofriendly. Most of the time the source for this approach was plant parts. In biological method,

green synthesis plays a noteworthy job [13–15]. In this study, we prepared Nickel oxide nanoparticles (NiO NPs) by eco-friendly method. Nickel being a transition metal it has a good anti-corrosion property. NiO NPs can be used as catalyst due to its high positive charge [16–19]. NiO NPs have lot of applications in pharmaceutical industries, biosensor, bio molecular separation, magnetic biocatalysts preparation, etc. [20–23]. Already some of the researchers reported that NiO NPs are used in carbon nanotubes because of their high electrical conductivity [24].

We utilized CGL as our green source to synthesis NiO NPs. *C. gigantea* belongs to the family of Apocynaceae and sub-family of Asclepiadoideae. The CGL consists of various secondary metabolites which can play a role as capping and stabilizing agent in the formation of metal nanoparticles [25,26]. This *C. gigantea* latex acts as an eco-friendly capping agent which can cap and produce highly stable metal oxide nanoparticles. Not only the latex but also the fibre from the plant also has certain specialities because of which it can be used in various nanoparticles synthesis.

In the view of applications, the synthesized nanoparticles have different contributions in day to day life. One of the major application was said to be catalytic property, which is essential for many organic transformations. NiO NPs were used in Ni-MH batteries which in turn

* Corresponding author.

E-mail address: mohanaroopan.s@vit.ac.in (S.M. Roopan).

¹ Equally contributed in this research work.

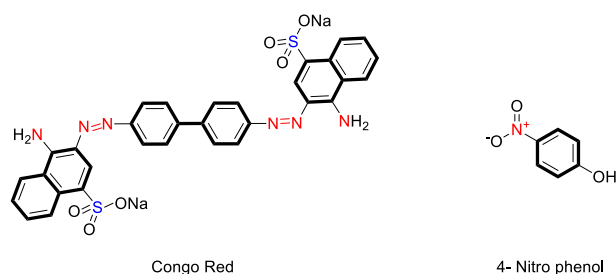


Fig. 1. Structure of Congo red and 4-nitrophenol.

is a reversible power source and pollution free. These eco-friendly synthesized nanoparticles have ability to act as catalyst in various organic applications and biological applications like antimicrobial, antitoxic, larvicidal, etc. [24,27]. CR was said to be one of the toxic diazo dye with two sulphur groups in structure (Fig. 1). Most of the industries released their toxic effluents directly or indirectly to the environment which leads to degrade the potency of natural resources [28]. To overcome this drawback, this report discuss on eco-friendly synthesis of NiO NPs, degradation of CR and nitrophenol.

2. Experimental section

2.1. Materials used

All the required compounds were obtained from Alfa Aesar, Mumbai, India. The *Calotropis gigantea* latex was collected from in and around Vellore Institute of Technology, Katpadi region, Vellore district, Tamilnadu, India and its co-ordinates are 12.9693° N and 79.1559° E.

2.2. CGL purification

CGL was separated into liquid and solid by adding 13 mL of CGL with 13 mL of distilled water and subjected for centrifugation (30 min @ 3000 rpm). Further the supernatant were thrown away and process was repeated once again to obtained clear product of CGL. Then 100 mg of the hardened mixture of CGL was diffuse in 100 mL of double distilled water (DD-H₂O) using ultrasonication and the resultant CGL

Table 1

Independent variables and there levels utilized in BBD model.

S. no	Variables	Range of values and levels		
		−1	0	1
1	Nickel acetate (mM)	0.5	1	1.5
2	Time (h)	3	4	5
3	Temperature (°C)	50	60	70

were deposited in refrigerator. Further the confirmation of CGL constituents were characterized by GC–MS analysis.

2.3. CGL mediated NiO NPs synthesis

Around 80 mL of 1 mM Nickel acetate solution was prepared using DD-H₂O and labelled (Solution-A). Solution B was prepared by adding 20 mL of DD-H₂O to 20 mg of CGL. Finally both the solutions were shaken well and kept in water bath at 60 °C for 4 h. Every 30 min intervals the mixture of sample solutions were collected and subjected to UV–Visible spectroscopy. The resultant solutions were centrifuged for 30 min at 3000 rpm. Further supernatant was discarded and calcinated with the help of crucible and furnace at 400 °C for 3 h [29]. Then the resultant powder was stored in a refrigerator for further elucidation. The reaction between Nickel acetate solution and CGL latex was explained in Fig. 2. The constituents present in latex can act as a capping agent to form NiO NPs.

2.4. Experimental modelling for optimization of NiO nanoparticles

Response surface methodology (RSM) was considering as one of the important modelling tools for optimizing various reaction parameters. Here we used, BBD (Box-Behnken Design) modelling for the synthesis of NiO NPs. The three independent variables for optimize the parameters (S_1 , S_2 , S_3) were selected as, Nickel acetate concentration (mM), Time (h), and Temperature (°C) in Table 1. The present study investigated about, 15 run of different combination of parameters (Table 2). The synthesis of NiO NPs results were fitted through following 2nd-order equation (Eq. (1))

$$\text{Abs (nm)} = \beta_0 + \beta_1 S_1 + \beta_2 S_2 + \beta_3 S_3 + \beta_{11} S_1^2 + \beta_{22} S_2^2 + \beta_{33} S_3^2 + \dots \quad (1)$$

Here Abs denotes absorption maximum, β_0 denotes constant, β_1 , β_{11} , β_2 , β_{22} , β_3 , β_{33} denotes both linear and quadratic coefficients.

Table 2

The experimental parameters for BBD design along with theoretical values.

Std order	Run order	Pt type	S_1	S_2	S_3	Abs max	
						Experimental	Theoretical
9	1	2	0	−1	−1	0.54	0.51
3	2	2	−1	1	0	0.78	0.78
13	3	0	0	0	0	1.25	1.25
14	4	0	0	0	0	1.25	1.25
8	5	2	1	0	1	1.02	1.01
5	6	2	−1	0	−1	0.62	0.62
12	7	2	0	1	1	0.94	0.96
2	8	2	1	−1	0	0.72	0.71
11	9	2	0	−1	1	0.75	0.76
7	10	2	−1	0	1	0.81	0.77
15	11	0	0	0	0	1.25	1.25
10	12	2	0	1	−1	0.78	0.76
4	13	2	1	1	0	0.99	0.97
1	14	2	−1	−1	0	0.56	0.58
6	15	2	1	0	−1	0.68	0.71

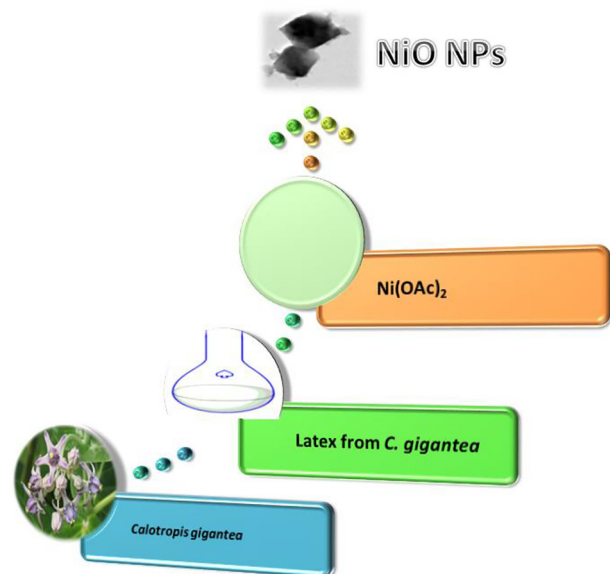
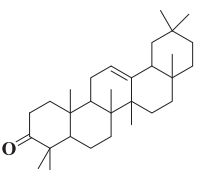
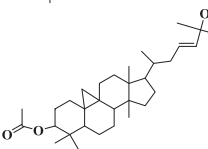
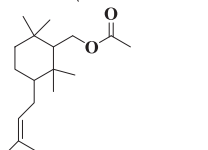


Fig. 2. Preparation of NiO NPs by CGL.

Table 3GC–MS profiling in *Calotropis gigantea latex* (CGL).

S. no	Retention time	Name of the compound	Molecular formula	Chemical structure
1.	28.57	4,4,6a,6b,8a,11,11,14b-Octamethyl-1,4,4a,5,6,6a,6b,7,8,8a,9,10,11,12,12a,14,14a,14b-octadecahydricen-3(2H)-one	C ₃₀ H ₄₈ O	
2.	28.89	(E)-3-(6-hydroxy-6-methylhept-4-en-2-yl)-2a,5a,8,8-tetramethyltetradecahydro-1H,12H-cyclopenta[a]cyclopropa[e]phenanthren-9-yl acetate	C ₃₂ H ₅₂ O ₃	
3	29.11	(2,2,6,6-Tetramethyl-3-(3-methylbut-2-en-1-yl)cyclohexyl)methyl acetate	C ₁₈ H ₃₂ O ₂	

2.5. Characterization techniques

Phase identification of CGL mediated NiO NPs was carried out using an X-ray diffraction method, company Bruker, Germany, model D8 in the 2θ range from 10 to 80°. The TEM (transmission electron microscopy) figures were attained on a Philips, CM 200, operating at 20–200 kV and resolution: 2.4 Å. Energy-dispersive X-ray spectroscopy (EDX) was obtained on the Bruker, Germany instrument. UV–Visible (UV–Vis) absorption spectra were acquired with a Shimadzu UV–Visible spectrophotometer, model UV 1800. The zeta potential of the CGL mediated NiO NPs was measured using Horiba Scientific. Brunauer–Emmett–Teller (BET) technique was utilized to identify the surface area of the NiO NPs. Perkin Elmer GCMS instrument was used to identify the constituent present in CGL.

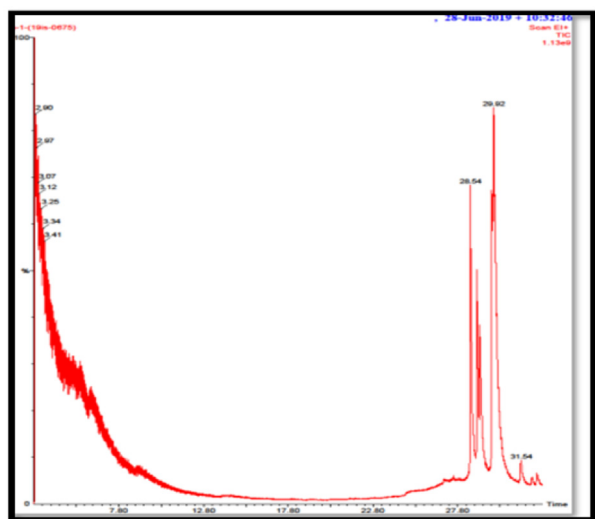
2.6. Degradation of azo dye by CGL mediated NiO NPs

Photocatalytic performance of CGL mediated NiO NPs were evaluated by the degradation of CR. About 0.1 g of NiO NPs was dissolved in 100 mL CR solution (10 mg/L) in each experiment. Prior to

photocatalytic measurements, the photocatalyst was pre-treated in darkness (30 min) to reach desorption–adsorption equilibrium of CR. After irradiation at particular time intervals, 3 mL of the solution was removed and centrifuged to separate the particles of photocatalyst. The concentration change in CR was examined on UV–Vis absorption of the suspensions at its peak absorbency at 520 nm. The cycling experiment was done under sunlight to test the reusability and photocatalytic stability of the optimized catalyst. The catalyst used in the reaction was washed and filtered thoroughly with DD-H₂O. Fresh CR solution was added to the used catalyst and repeated the experiments for several times.

2.7. Catalytic reduction of 4-nitrophenol

The photo catalytic degradation of 4-nitrophenol was performed in 5×10^{-5} M solution with the combination of NiO NPs (50 mg), and 4-nitrophenol (50 mL). The control reactions were carried out in the absence of catalyst. All experiments were performed using identical conditions. The adsorption equilibrium took place at the first 5 min of every run. The degradation of 4-nitrophenol was examined via disappearance of corresponding 400 nm absorption peak acquired by progressive UV–Visible data.

**Fig. 3.** GC–MS chromatogram of CGL latex.**Table 4**

ANOVA for synthesis of NiO NPs.

Source	DF	Adj SS	Adj MS	F-value	p-Value
Model	9	0.829593	0.092177	94.06	0.000
Linear	3	0.258250	0.086083	87.84	0.000
S ₁	1	0.051200	0.051200	52.24	0.001
S ₂	1	0.105800	0.105800	107.96	0.000
S ₃	1	0.101250	0.101250	103.32	0.000
Square	3	0.564468	0.188156	192.00	0.000
S ₁ * S ₁	1	0.193206	0.193206	197.15	0.000
S ₂ * S ₂	1	0.247206	0.247206	252.25	0.000
S ₃ * S ₃	1	0.210467	0.210467	214.76	0.000
2-Way interaction	3	0.006875	0.002292	2.34	0.190
S ₁ * S ₂	1	0.000625	0.000625	0.64	0.461
S ₁ * S ₃	1	0.005625	0.005625	5.74	0.062
S ₂ * S ₃	1	0.000625	0.000625	0.64	0.461
Error	5	0.004900	0.000980		
Lack-of-fit	3	0.004900	0.001633		
Pure error	2	0.000000	0.000000		
Total	14	0.834493			

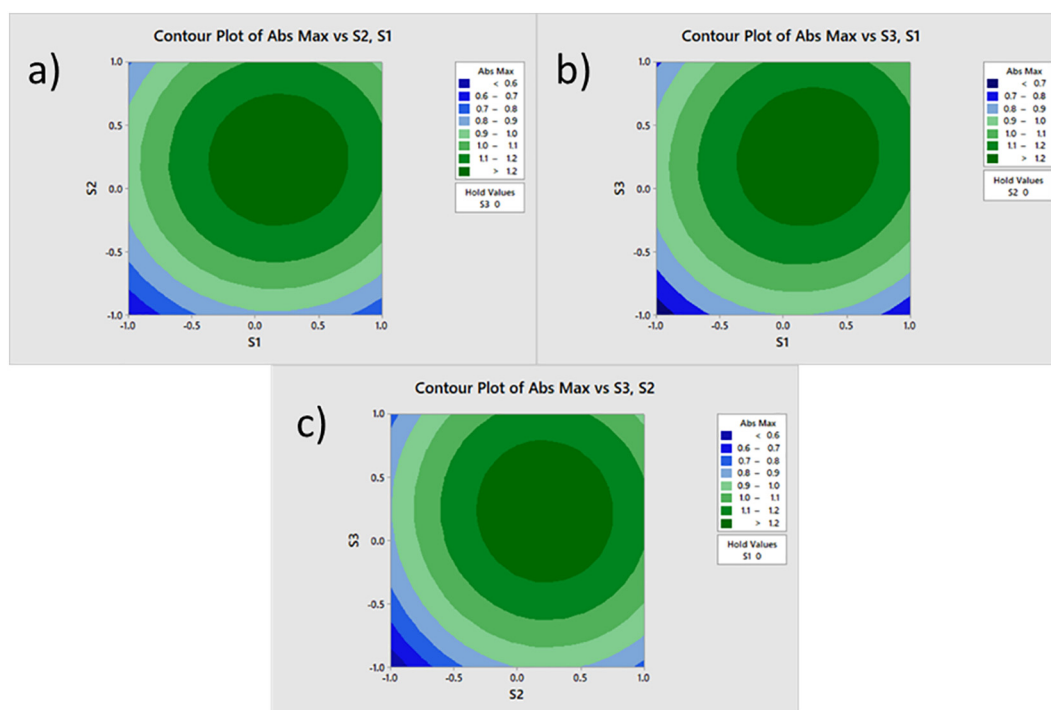


Fig. 4. The 2D contour plots for all independent variables a) S_2 Vs S_1 b) S_3 Vs S_1 c) S_3 Vs S_2 .

3. Results and discussion

3.1. GC-MS analysis of CGL

Bioactive compounds present in CGL were investigated via GCMS analysis. From that GC-MS chromatogram, we confirmed that the existence of phytochemical components with various retention times as presented in Table 3. Fig. 3 represented that the

chromatogram of CGL latex. The current study finds to predict the molecular formula and structure of the three bioactive components.

3.2. The RSM and ANOVA analysis

The preparation of NiO NPs was investigated using RSM methodology. The BBD experimental runs were calculated and presented in

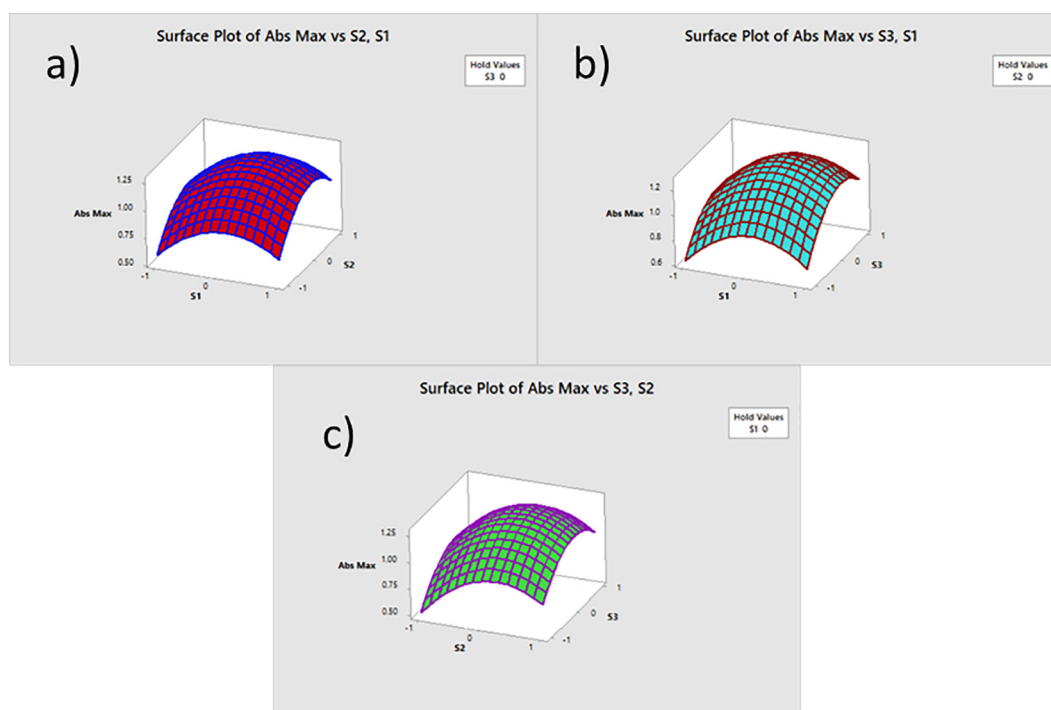


Fig. 5. The 3D surface plots for all independent variables a) S_2 Vs S_1 b) S_3 Vs S_1 c) S_3 Vs S_2 .

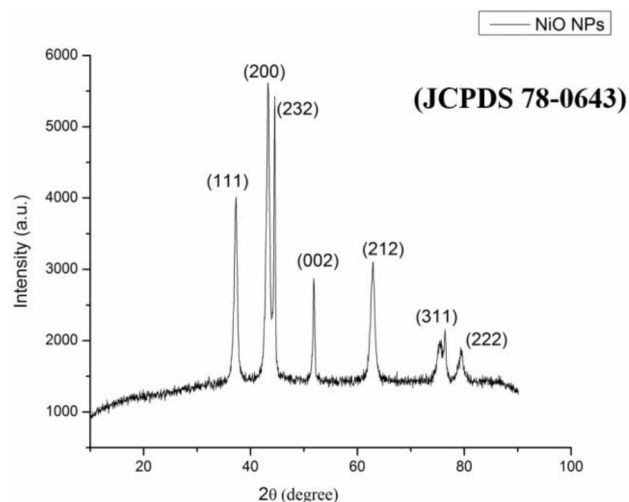


Fig. 6. XRD spectrum of CGL mediated NiO NPs.

Table 2, according to the table values the 2nd order regression equation (2) for three independent parameters,

$$\begin{aligned} \text{Abs Max} = & 1.2500 + 0.0800 S_1 + 0.1150 S_2 + 0.1125 S_3 - 0.2288 S_1 \\ & * S_1 - 0.2587 S_2 * S_2 - 0.2388 S_3 * S_3 + 0.0125 S_1 * S_2 \\ & + 0.0375 S_1 * S_3 - 0.0125 S_2 * S_3 \end{aligned}$$

The ANOVA Table 4, investigated for the significance and adequacy of the present model. From this table, F-value (252.25) and *p*-value (<0.001) represents the model should be high significant. The *R*² value of the current model was 99.41% and *R*² (adj) was 98.36 %. Both values represents the model should be highly adequate and significant. Meanwhile, the 2D and 3D plots (Figs. 4(a–c) & 5(a–c)) are used for identify the adequacy of the model. It can be observed that, RSM analysis illustrate that the interaction between two indexes, nickel acetate (*S*₁) and Time (*S*₂) as well as nickel acetate (*S*₁) and Temperature (*S*₃) are significant. Finally the best optimum condition was identified as 1 mM of nickel acetate, 4 h time and 60 °C. It is also confirmed by experimental results.

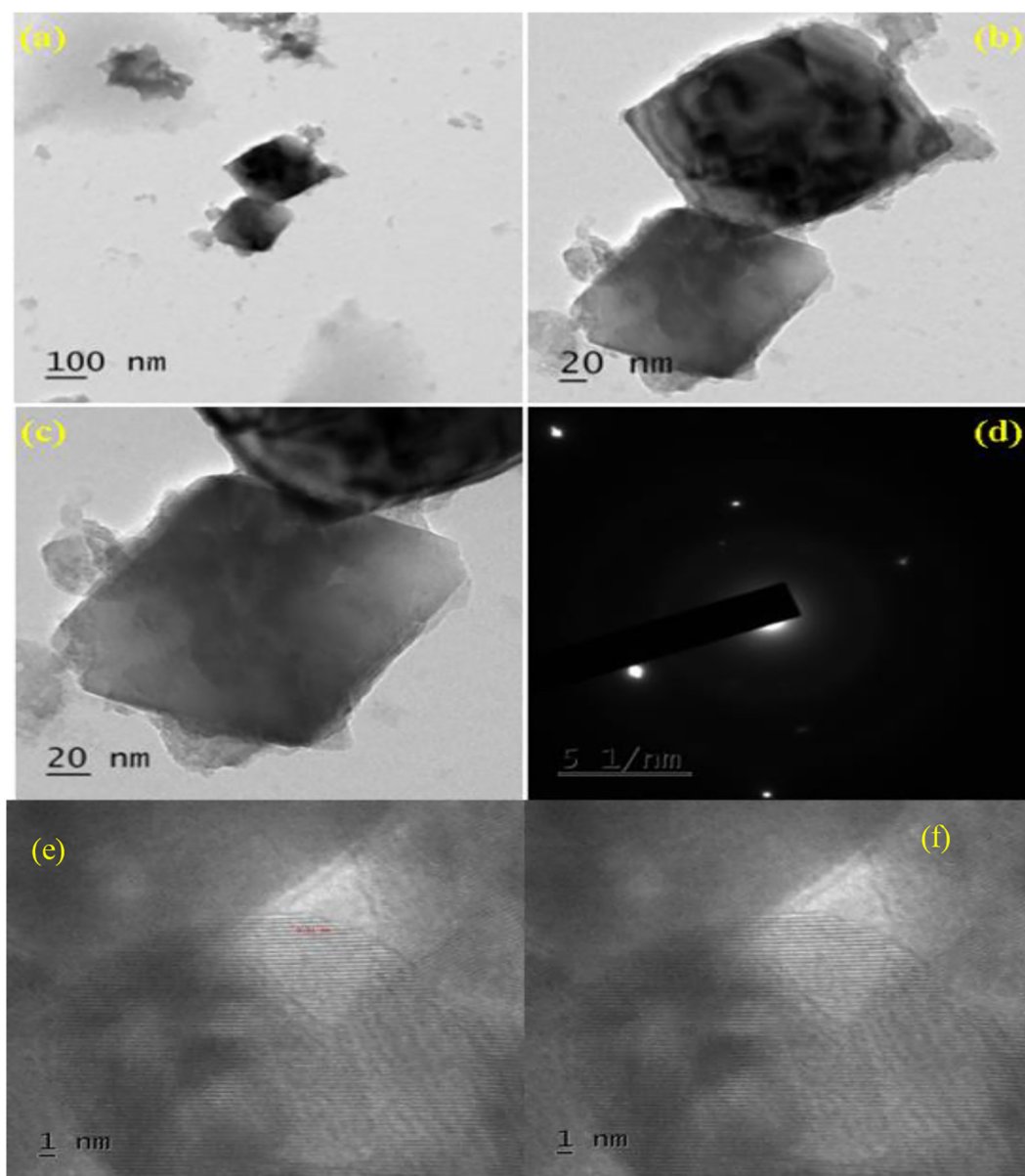


Fig. 7. (a–c) TEM images of CGL mediated NiO NPs, d - SAED pattern of CGL mediated NiO NPs (e–f) fringes of NiO.

Table 5
Comparative methodology for Green synthesis.

S. no	Methodology	Particle size	References
1.	Hot-injection method.	100 nm	[41]
2.	Sol-gel method	32.9 nm.	[42]
3.	Thermal oxidation	30 nm	[43]
4.	Thermal decomposition	62 ± 1 nm	[44]
5.	Thermal decomposition.	55 nm	[45]
6.	Green synthesis	24 nm	Current study

3.3. XRD data

NiO NPs formation was determined by X-ray diffraction which shown in Fig. 6. All the diffraction peaks can be unequivocally assigned to face-centered cubic phase of NiO [29]. The lattice constant of CGL mediated NiO NPs from XRD spectrum was found to be $a = 4.1769 \text{ \AA}$, which is good agreement with JCPDS 78-0643 [30]. Five broad characteristic peaks located at 37.2° , 43.29° , 62.91° , 75.43° and 79.38° can be indexed respectively to the (111), (200), (220), (311) and (222) planes. The average crystalline size was calculated from the Debye Scherrer's Equation [31,32] to be around 29 nm, which was consistent with the results of TEM.

3.4. Morphological analysis of NiO NPs

Fig. 7(a–c) confirmed the TEM photographs of NiO NPs synthesized via CGL extract. The synthesized single-crystalline cubic CGL mediated NiO NPs showed regular hexahedral in shape and uniform in size distribution [33]. Sizes of the NiO NPs were differing from 20 to 100 nm, with a common of 24 nm and the presence of some large aggregates. Fig. 7d illustrates the SAED pattern indicating the single and highly crystalline structure of CGL mediated NiO NPs. Compare to all other chemical methods, the CGL mediated NiO NPs showed excellent crystalline nature and lesser particle dimension in Table 5. Moreover, chemical composition evaluation performed using energy dispersive X-ray spectroscopy (EDS). The EDS spectra of the CGL mediated NiO NPs (Fig. 8) showed the presence of C, O, Ni and the content of C, O, Ni are 3%, 14%, and 83% respectively. Furthermore, we complemented the particle size of CGL mediated NiO NPs by Diffused Light scattering (DLS) technique. As shown in Fig. 9, the CGL mediated NiO NPs were formed and resulted in -53.5 mV , which is in agreement with the particle

Calculation Results

Peak No.	Zeta Potential	Electrophoretic Mobility
1	-53.5 mV	-0.000277 cm ² /Vs
2	---	---
3	---	---

Zeta Potential (Mean) : -53.5 mV
Electrophoretic Mobility Mean : -0.000277 cm²/Vs

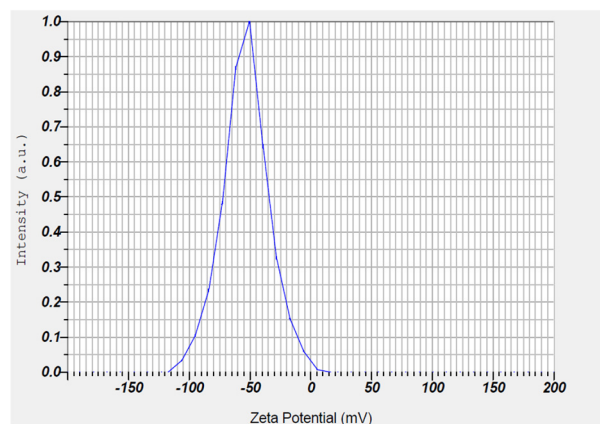


Fig. 9. Zeta potential of synthesized CGL mediated NiO NPs.

size distribution given by a Horiba Scientific dynamic light scattering analysis.

3.5. UV-Visible spectroscopy

The UV-Vis peaks of CGL modified NiO NPs were studied at different time intervals as represented in Fig. 10. The absorption band was appeared in the range of 225–275 nm (Fig. 10). It was likely correlated to the sufficient peak development of CGL mediated NiO NPs at 120 min [34]. From UV image, the intensity of peaks was minimized also detected in lower wavelength, which specifies the interactions between CGL extract and NiO. The conventional Tauc's relation $[(\alpha h\nu)^{1/n} = A(h\nu - E_g)]$ was utilized to find the band gap. Whereas $h\nu$ denotes as the incident photon energy, 'A' denotes as a constant, and 'n' denotes exponential value [35,36]. By extrapolating the intercept at $\alpha = 0$ of the graph of $(\alpha h\nu)^2$ Vs $h\nu$ the E_g value can be determined. The obtained E_g value is 2.7 eV [29] for the CGL mediated NiO NPs at 120 min.

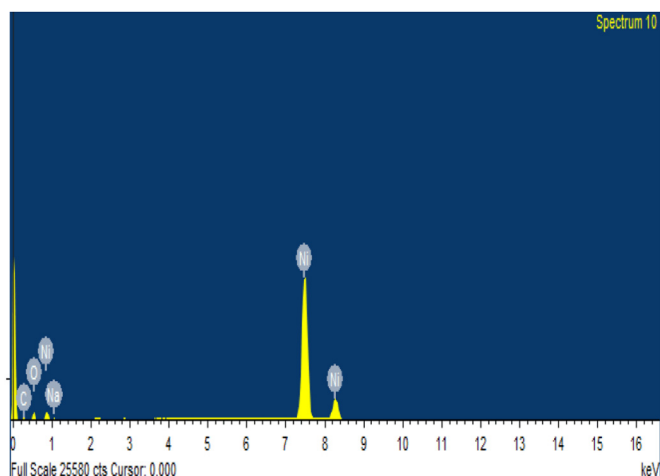


Fig. 8. EDS spectrum of CGL mediated NiO NPs.

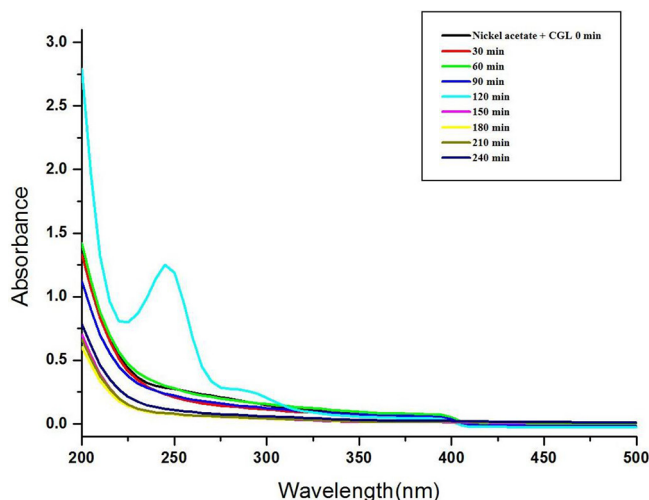


Fig. 10. UV-Visible spectra of CGL mediated NiO NPs.

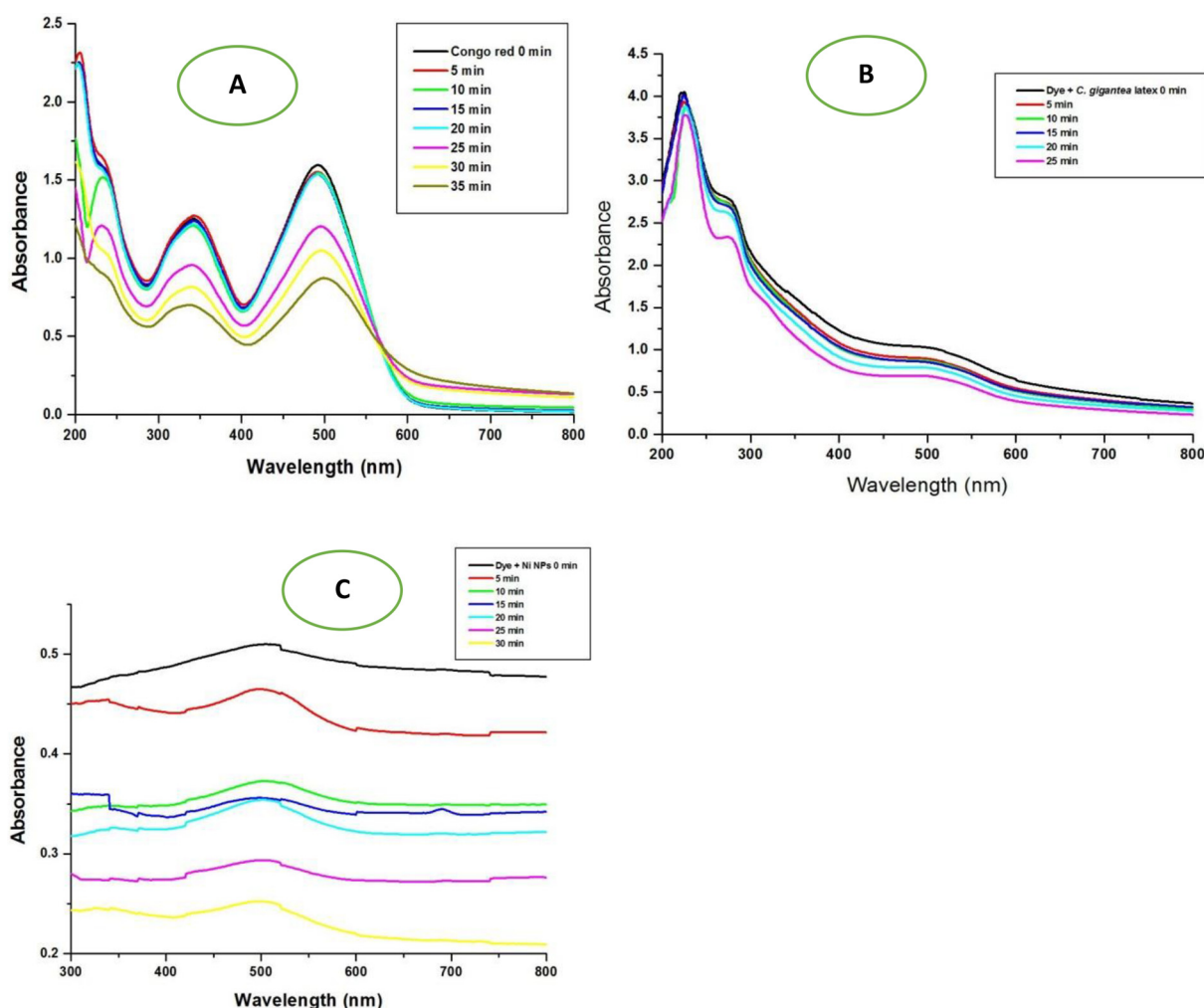


Fig. 11. UV-Vis spectra of CR degradation: a) In presence of NiO photocatalyst, b) In presence of CGL Cextract, c) In presence of CGL mediated NiO photocatalyst.

3.6. Photocatalytic degradation of Congo red

Degradation of environmental contaminants under suitable conditions i.e., using solar spectrum in aqueous solution is the aim of this application. To evidence this photocatalytic performance, as a trial reaction the photocatalytic decomposition of CR was performed according to the literature [28,39]. Photocatalytic activity tests were done, on adding catalysts to an aqueous CR solution (Fig. 11(a-c)), the resulting suspensions were equilibrated in the dark for 30 min, and the suspensions were irradiated with the sun light for 35 min. The adsorption of CR on the CGL mediated NiO NPs under dark was insignificant. As mentioned in earlier work, experiment in dark and without photo catalyst does not remove the CR dye notably. Only small change in the concentration of the solution can be observed when CR solution was irradiated in dark and in the absence of any catalyst. After 35 min of irradiation under sunlight, the degradation ratio of CR was 95 % (Fig. 11c) in the presence of CGL mediated NiO NPs whereas, 36 % (Fig. 11a) and 28 % (Fig. 11b) of CR were decomposed by NiO and CGL extract respectively. Therefore, we envision that the superior photocatalytic activity for catalyst can be obtained because of the existence of CGL mediated NiO NPs. The catalytic activity also compared with P25 [37] CR dye degradation exhibited that 91.5 % was obtained in the existence of Ba/Alg/CMC/TiO₂ composite. Also Bhagwat et al. [38] reported the MgTiO₂-P25 showing 98 % of degradation of CR in 120 min. Ullah et al. [39] also reported that W@TiO₂

nanoparticles can be a low-cost preference for visible light induced photocatalytic degradation of CR dye.

The kinetic behaviour was carried out to further elucidate the photocatalytic activity. As shown in Fig. 12(a-d), the plots of CR dye decomposition matched the pseudo-first order kinetic correlation [40]. The kinetic expression can be presented as follows (1):

$$\ln\left(\frac{C}{C_0}\right) = -k_{app}t$$

where, C denotes the CR dye concentration at initial t (mg/L); C₀ denotes the CR dye concentration at t = 0 (mg/L); k_{app} also denotes the pseudo first-order rate constant (min⁻¹); and t denotes the time of reaction (min). Evidently, the result for CGL mediated NiO NPs (0.9027) was the highest among all the other samples, which was consistent with the conclusion of photocatalytic degradation. To check the stability of the CGL mediated NiO NPs in the process of photocatalytic activity, we also carried out repeated photodegradation of CR dye experiments. The results shows that the photocatalytic efficiency of the CGL mediated NiO NPs during CR degradation was significantly higher.

3.7. BET surface area measurements

The photocatalytic behaviour of the materials was mainly based on the amount of the pore in their surface, which was investigated using

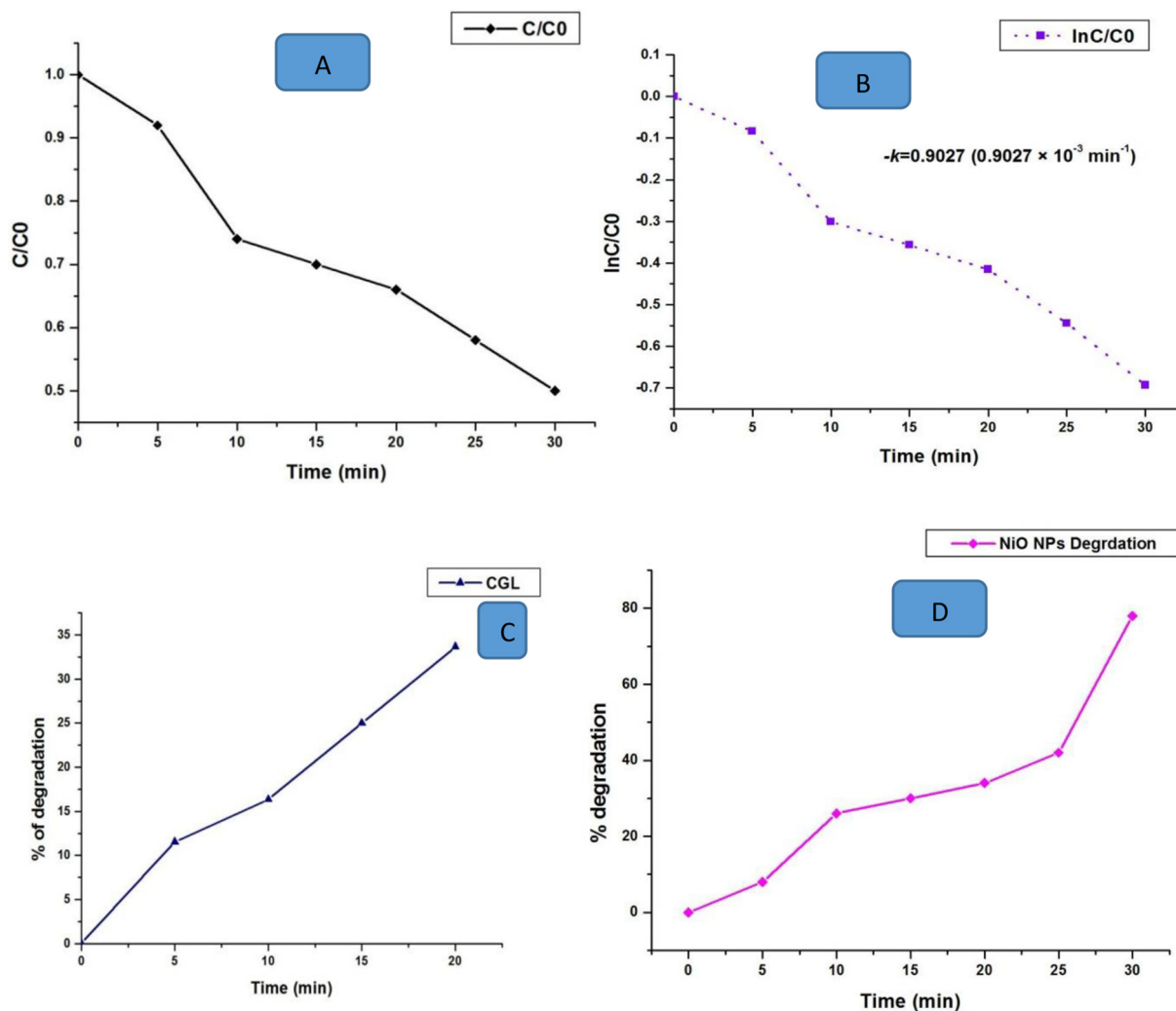


Fig. 12. Photocatalytic degradation curves of CR dye: a) Degradation rate curve in presence of NiO photocatalyst, b) Degradation kinetics in presence of NiO photocatalyst, c) Degradation efficiency in presence of CGL C extract, d) Degradation efficiency in presence of CGL mediated NiO NPs.

BET analysis. Here synthesis of NiO NPs was calcinated at 300 °C for 1 h due to the removal of water and other organic pollutants. At constant temperature of 77 K the NiO NPs were analysed via them to absorb nitrogen gas. As adsorption occurs, until it attains equilibrium, the pressure in the sample varies. Further surface area was found out using following equation

$$\frac{P/P_0}{V\left(1-\frac{P}{P_0}\right)} = \frac{1}{cV_m} + C - \frac{1}{cV_m} \left(\frac{P}{P_0}\right)$$

Here

P - represents as the equilibrium pressure

P₀ - represents the equilibrium and saturation pressures of the adsorbed gas,

P/P₀ - represents the relative pressure,

V - denotes volume of adsorbed gas per kg adsorbent,

V_m - denotes volume of monolayer adsorbed gas/kg adsorbent, and

c - Denotes the constant from the heat

The BET (N₂ adsorption/desorption isotherm) analysis of NiO nanoparticles was exhibit in Fig. 13. Surface area of NiO NPs, was obtained as 11.248 m²/g respectively. Total pore volumes for pores 0.456 cm³/g

with radius of 5.863e−03 cm³/g are calculated for NiO NPs employing a Barret-Joyner-Halenda (BJH) model. From, this analysis we identified that the surface area increases in NiO content.

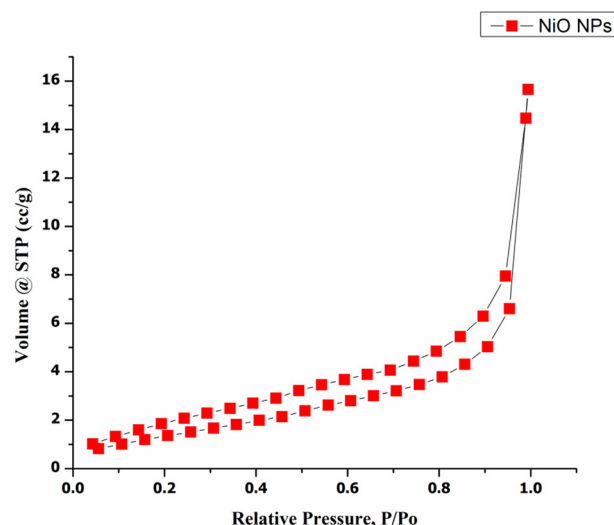


Fig. 13. BET analysis for NiO NPs.

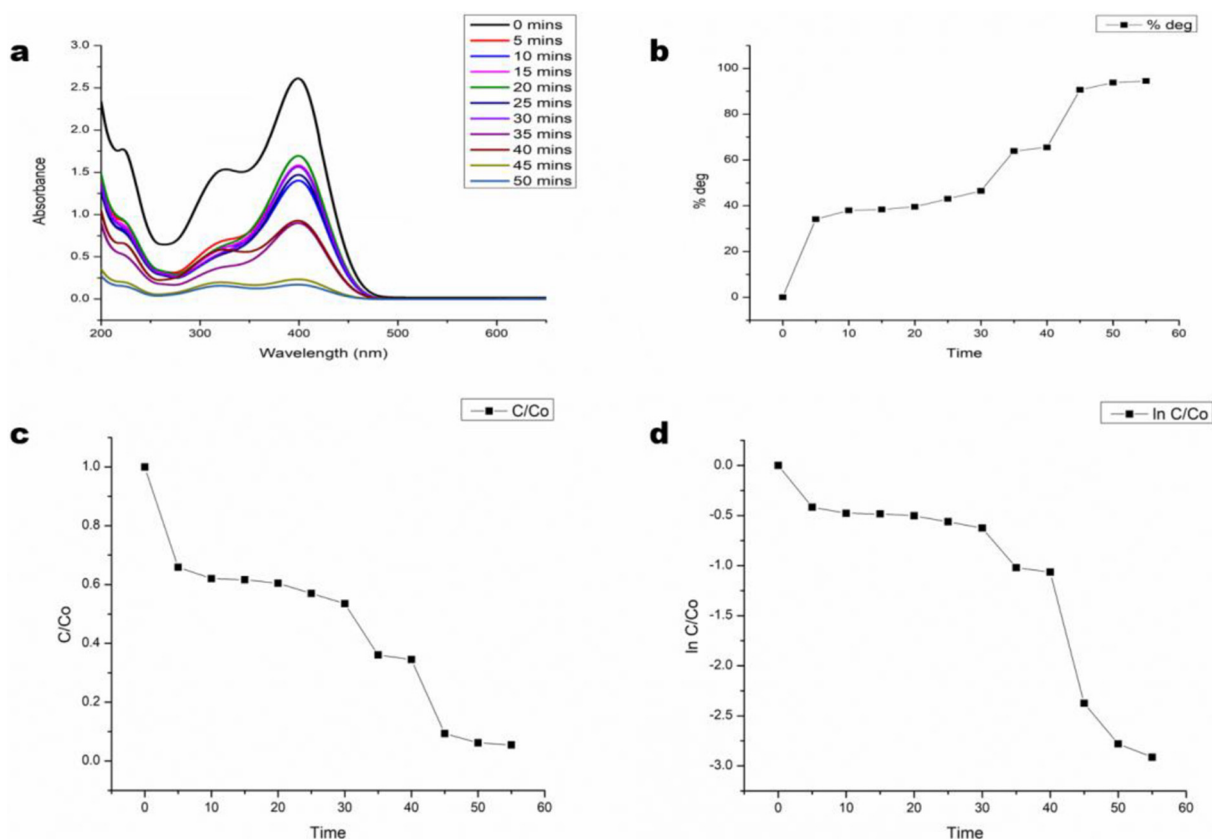


Fig. 14. (a) Photo catalytic degradation of 4-nitro phenol. (b–d) Kinetic graphs for degradation of 4-nitro phenol.

3.8. Catalytic activity of 4-nitro phenol

The photo catalytic process was observed utilizing UV–Vis spectrophotometry as exhibited in Fig. 14(a–d). The 4-Nitrophenolates ions were once obtained in excessive absorption peak placed at 400 nm.

Subsequently, emerging the nanoparticles, current absorption peak constantly declined throughout the path of reaction. After 50 min of the reaction time, the 400 nm absorption peak was absolutely vanished. The conversion of 4-nitrophenol to 4-aminophenol, indicates that look of new and weak peak at 290 nm. The kinetic plots are shown in

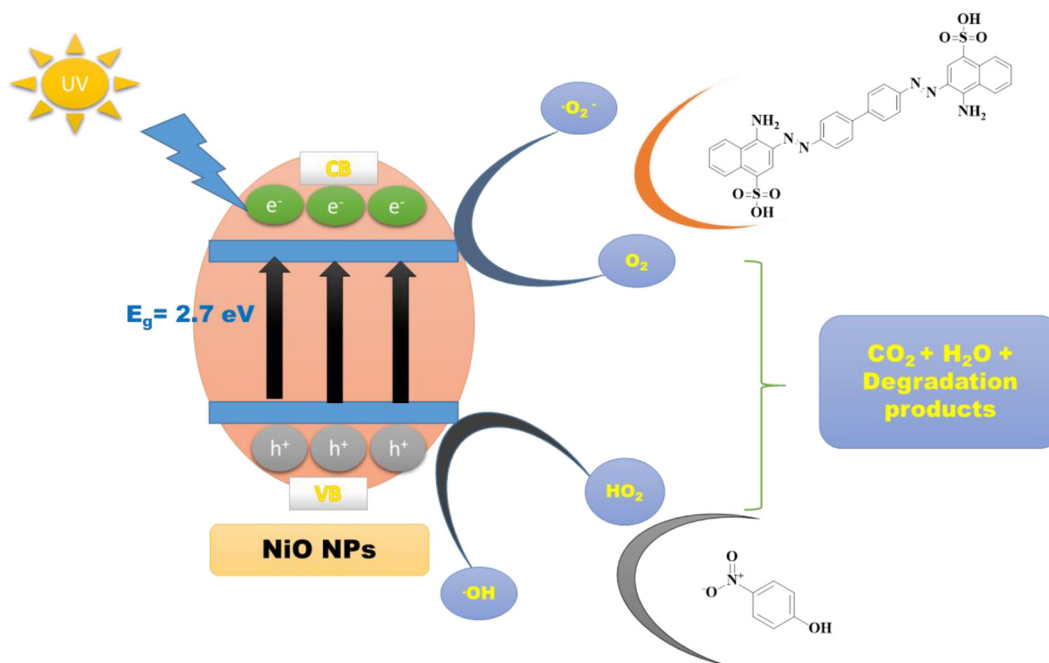


Fig. 15. Photocatalytic degradation mechanism of CR and 4-nitro phenol over NiO NPs under visible light.

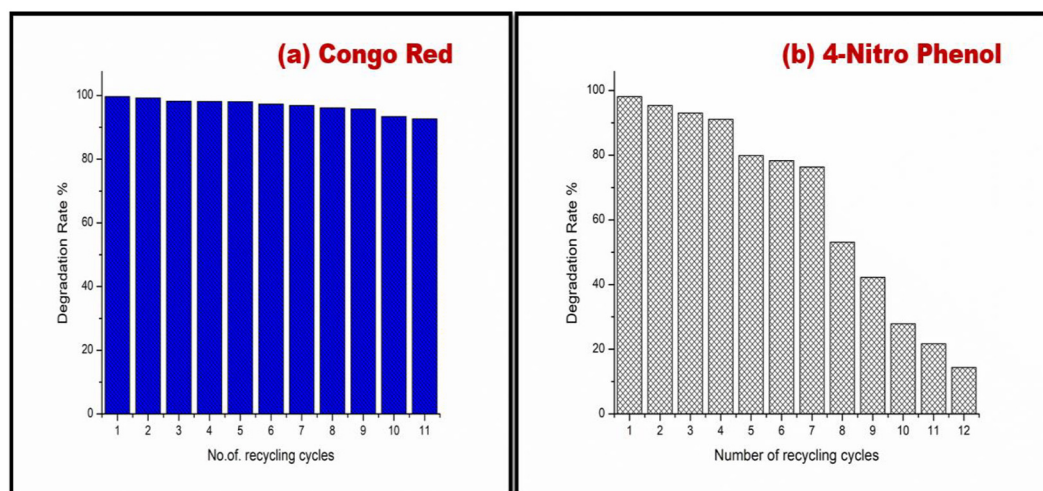


Fig. 16. (a & b) Recyclability of NiO NPs for catalytic activity of CR dye and 4-nitro phenol.

Table 6
BET analysis for photocatalytic degradation.

NiO NPs/dye	Before degradation		After degradation	
	Surface area	Pore volume	Surface area	Pore volume
Congo red	11.248 m ² /g	0.426 cm ³ /g	3.540 m ² /g	0.194 cm ³ /g
4-Nitro phenol	11.248 m ² /g	0.426 cm ³ /g	4.955 m ² /g	0.137 cm ³ /g

Fig. 14(b–d). From the kinetic analysis, we found that 94% degradation of 4-nitro phenol occurs in 50 min. It also follows a pseudo-first order reaction. It was beneficial to make reference to that in the absence of the NiO NPs; there was no significant modification in position and/or intensity of the peak due to the 4-nitrophenolate ion. Specifically, the reduction of 4-nitrophenolate ion to 4-aminophenol was unable to perform in control experiments. It was known that, NiO NPs to be a strong reducing agent.

3.9. Mechanism of photocatalytic degradation

The several steps containing possible mechanism for sunlight mediated degradation of CR was shown in Fig. 15. From the initial step, the light energy was irradiated on the semiconductor, then valance band electrons absorbs energy and shifts to the conduction band. Consequently the charge bearers (hole in the valence band and electrons in the conduction band) are produced. In the following stage, the dye material & organic material are directly interact with these generated charge carriers to degrade them or transfer to the semiconductor surface. Further, these primary materials are degrade/reduce, go on

secondary reactions. The resultant products, are free radicals like $\cdot\text{OH}$, HO_2 , O_2^- . Then the free radicals also degrade/reacts them to produce non-toxic products. The band gap of the NiO NPs was 2.7. From this above possible mechanism, the organic pollutant CB electrons are transfers highly into VB, and then degraded.

3.10. Reusability of NiO NPs

The reusability was one of the significant factors for feasible application. Fig. 16 (a & b) represents that the reusability of the NiO as a photo catalyst for degradation of CR & 4-nitrophenol. Thus the reusable cycle test was accomplished for NiO NPs under UV light for 10 cycles. Each time, the photo catalyst used to be re-utilized as fresh catalyst for the following cycles of photocatalytic experiment. After the 10th cycles photo degradation result was observed that the photo catalyst was still stable. It was further supported by BET analysis. In CR dye has its maximum efficiency (photo degradation rate 92.6 % of and above) and for 4-nitrophenol has moderate efficiency in all the 10 cycles.

3.11. Surface area study for after degradation

The NiO NPs surface area performs a vital role in photocatalytic degradation reactions. Before and after the photocatalytic reactions, the pore volume, pore diameter, and surface area of synthesized NiO NPs were presented in Table 6. It can be noticeably spotted that N_2 isotherm of NiO NPs for photo catalytic degradation, which confirmed pore volume decreased, and surface area increased.

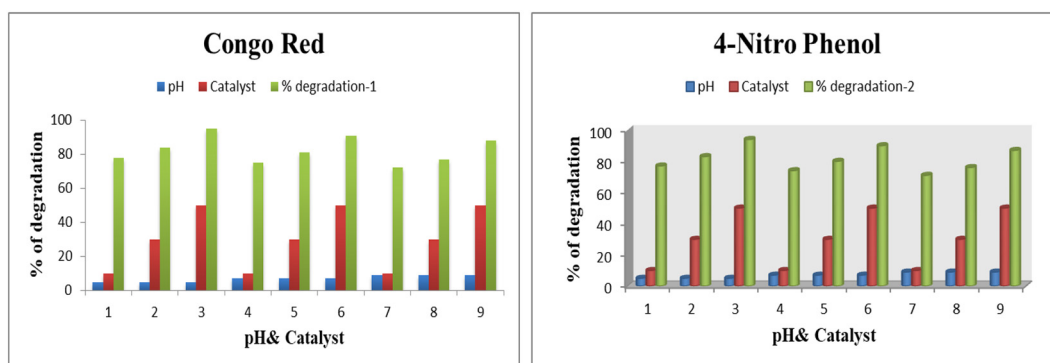


Fig. 17. Effect of pH and catalyst.

3.12. Influence of pH and NiO catalyst on degradation studies

The photo catalytic degradation of CR dye and 4-nitro phenol investigated using NiO NPs as a catalyst. In degradation studies, the amount of catalyst and pH also considerable as one of the important factor. To optimize the parameters we have changed the catalyst quantity (10, 30, and 50 mg), and pH of the solution (5, 7, and 9). Same parameters applied in both CR and 4-nitro phenol degradation studies. It was observed that while increasing the catalyst, % of degradation also increased. Also, the pH at acidic condition (pH = 5) showing good degradation efficiency. Fig. 17 represents the effect of the pH and catalyst in both degradation studies. It was interesting that the no considerable change in both degradation studies.

4. Conclusion

In summary, we have developed a CGL mediated NiO NPs by eco-friendly method without using any hazardous chemicals. The degradation study results revealed that CGL mediated NiO NPs shows considerably enriched photocatalytic activity.

References

- [1] R.K. Jha, P.K. Jha, K. Chaudhury, S.V.S. Rana, S.K. Guha, An emerging interface between life science and nanotechnology: present status and prospects of reproductive healthcare aided by nano-biotechnology, *Nano Rev.* 5 (2014), 22762. <https://doi.org/10.3402/nano.v5.22762>.
- [2] L. Liu, Emerging Nanotechnology Power, World Scientific, 2009 <https://doi.org/10.1142/7224>.
- [3] C.L. Keat, A. Aziz, A.M. Eid, N.A. Elmarzugi, Biosynthesis of nanoparticles and silver nanoparticles, *Bioresour. Bioprocess.* 2 (2015) <https://doi.org/10.1186/s40643-015-0076-2>.
- [4] D. Sharma, S. Kanchi, K. Bissety, Biogenic synthesis of nanoparticles: a review, *Arab. J. Chem.* (2015) <https://doi.org/10.1016/j.arabj.2015.11.002>.
- [5] I. Khan, K. Saeed, I. Khan, Nanoparticles: properties, applications and toxicities, *Arab. J. Chem.* (2017) <https://doi.org/10.1016/j.arabj.2017.05.011>.
- [6] R.S. Geommonond, A.G.M. Da Silva, P.H.C. Camargo, Controlled synthesis of noble metal nanomaterials: motivation, principles, and opportunities in nanocatalysis, *An. Acad. Bras. Cienc.* 90 (2018) 719–744. <https://doi.org/10.1590/0001-3765201820170561>.
- [7] A. Gentile, F. Ruffino, M. Grimaldi, Complex-morphology metal-based nanostructures: fabrication, characterization, and applications, *Nanomaterials* 6 (2016) 110. <https://doi.org/10.3390/nano6060110>.
- [8] Y.X. Zhang, Y.H. Wang, Nonlinear optical properties of metal nanoparticles: a review, *RSC Adv.* 7 (2017) 45129–45144. <https://doi.org/10.1039/c7ra07551k>.
- [9] P.R. Sajjalal, T.S. Sreeprasad, A.K. Samal, T. Pradeep, Anisotropic nanomaterials: structure, growth, assembly, and functions, *Nano Rev.* 2 (2011) 5883. <https://doi.org/10.3402/nano.v2i0.5883>.
- [10] P. Singh, Y.J. Kim, D. Zhang, D.C. Yang, Biological synthesis of nanoparticles from plants and microorganisms, *Trends Biotechnol.* 34 (2016) 588–599. <https://doi.org/10.1016/j.tibtech.2016.02.006>.
- [11] M.A. Sabri, A. Umer, G.H. Awan, M.F. Hassan, A. Hasnain, Selection of suitable biological method for the synthesis of silver nanoparticles, *Nanomater. Nanotechnol.* 6 (2016) 29. <https://doi.org/10.5772/62644>.
- [12] J. Virkutyte, R.S. Varma, Green synthesis of nanomaterials: environmental aspects, *ACS Symp. Ser.* 1124 (2013) 11–39. <https://doi.org/10.1021/bk-2013-1124.ch002>.
- [13] Siavash Iravani, Green synthesis of metal nanoparticles using plants, *Green Chem.* 13 (2011) 2638–2650. <https://doi.org/10.1039/c1gc00145>.
- [14] S. Saif, A. Tahir, Y. Chen, Green synthesis of iron nanoparticles and their environmental applications and implications, *Nanomaterials* 6 (2016) 209. <https://doi.org/10.3390/nano6110209>.
- [15] G. Shobha, V. Moses, S. Ananda, Biological synthesis of copper nanoparticles and its impact, *Int. J. Pharm. Sci. Invent.* 3 (2014) 2319–6718. <https://doi.org/10.5101/nbe.v4i2.p99-106.1> ISSN.
- [16] F. Motahari, M.R. Mozdianfar, F. Soofivand, M. Salavati-Niasari, NiO nanostructures: synthesis, characterization and photocatalyst application in dye wastewater treatment, *RSC Adv.* 4 (2014) 27654–27660. <https://doi.org/10.1039/c4ra02697g>.
- [17] F. Tian, S. Liu, H. Tian, R. Dong, Y. Zhang, D. Wei, L. Ye, L. Whitmore, Growth and photocatalytic properties of NiO nanostructures prepared in acidic and alkaline solutions with same reagents, *J. Phys. Chem. C* 123 (2019) 504–510. <https://doi.org/10.1021/acs.jpcc.8b09384>.
- [18] F. Torki, H. Faghihian, Visible light degradation of naproxen by enhanced photocatalytic activity of NiO and NiS, scavenger study and focus on catalyst support and magnetization, *Photochem. Photobiol.* 94 (2018) 491–502. <https://doi.org/10.1111/php.12906>.
- [19] D. Yazdani, A.A. Zinatizadeh, M. Joshaghani, One-step synthesis of NiO nanophotocatalyst by wire explosion process and its application in photocatalytic degradation of methyl tert-butyl ether, *Water Environ. J.* (2018) <https://doi.org/10.1111/wej.12387>.
- [20] X. Meng, X. Zhang, Y. Bing, N. Xu, W. Shi, P. Cheng, In situ generation of NiO nanoparticles in a magnetic metal-organic framework exhibiting three-dimensional magnetic ordering, *Inorg. Chem.* 55 (2016) 12938–12943. <https://doi.org/10.1021/acs.inorgchem.6b02376>.
- [21] I.S. Lee, N. Lee, J. Park, B.H. Kim, Y.W. Yi, T. Kim, T.K. Kim, I.H. Lee, S.R. Paik, T. Hyeon, Ni/NiO core/shell nanoparticles for selective binding and magnetic separation of histidine-tagged proteins, *J. Am. Chem. Soc.* 128 (2006) 10658–10659. <https://doi.org/10.1021/ja063177n>.
- [22] P. Yang, X. Tong, G. Wang, Z. Gao, X. Guo, Y. Qin, NiO/SiC nanocomposite prepared by atomic layer deposition used as a novel electrocatalyst for nonenzymatic glucose sensing, *ACS Appl. Mater. Interfaces* 7 (2015) 4772–4777. <https://doi.org/10.1021/am508508m>.
- [23] C.A. Sousa, H.M.V.M. Soares, E.V. Soares, Nickel oxide (NiO) nanoparticles induce loss of cell viability in yeast mediated by oxidative stress, *Chem. Res. Toxicol.* 31 (2018) 658–665. <https://doi.org/10.1021/acs.chemrestox.8b00022>.
- [24] M. Gong, W. Zhou, M.C. Tsai, J. Zhou, M. Guan, M.C. Lin, B. Zhang, Y. Hu, D.Y. Wang, J. Yang, S.J. Pennycook, B.J. Hwang, H. Dai, Nanoscale nickel oxide/nickel heterostructures for active hydrogen evolution electrocatalysis, *Nat. Commun.* 5 (2014) <https://doi.org/10.1038/ncomms5695>.
- [25] C. Tamuly, I. Saikia, M. Hazarika, M. Bordoloi, N. Hussain, M.R. Das, K. Deka, Bio-derived ZnO nanoflower: a highly efficient catalyst for the synthesis of chalcone derivatives, *RSC Adv.* 5 (2015) 8604–8608. <https://doi.org/10.1039/C4RA14225J>.
- [26] U. Bora, R.K. Das, P. Sharma, P. Nahar, Synthesis of gold nanoparticles using aqueous extract of Calotropis procera latex, *Mater. Lett.* 65 (2011) 610–613. <https://doi.org/10.1016/j.matlet.2010.11.040>.
- [27] N. Saraswathy, V. Thirumurugan, Green synthesis of silver nanoparticles using Cassia glauca bark extract and its antibacterial activity, 20 (2016) 240–244.
- [28] S. Lan, L. Liu, R. Li, Z. Leng, S. Gan, Hierarchical hollow structure ZnO: synthesis, characterization, and highly efficient adsorption/photocatalysis toward congo red, *Ind. Eng. Chem. Res.* 53 (2014) 3131–3139. <https://doi.org/10.1021/ie404053m>.
- [29] M. Ramesh, M.P.C. Rao, S. Anandan, H. Nagaraja, Adsorption and photocatalytic properties of NiO nanoparticles synthesized via a thermal decomposition process, *J. Mater. Res.* 33 (5) (2018) 601–610. <https://doi.org/10.1557/jmr.2018.30>.
- [30] C. Xu, K. Hong, S. Liu, G. Wang, X. Zhao, A novel wet chemical route to NiO nanowires, *J. Cryst. Growth* 255 (2003) 308–312. [https://doi.org/10.1016/S0022-0248\(03\)01246-6](https://doi.org/10.1016/S0022-0248(03)01246-6).
- [31] R. Azimrad, P. Khosravi, A.Z. Moshfegh, Synthesis of W17047 nanothick plates with preferred orientation and their photocatalytic activity, *Surf. Interface Anal.* 43 (2011) 1397–1402. <https://doi.org/10.1002/sia.3730>.
- [32] M.A. Behnajady, Y. Tohidi, Synthesis, characterization and photocatalytic activity of mg-impregnated ZnO-SnO₂ coupled nanoparticles, *Photochem. Photobiol.* 90 (2014) 51–56. <https://doi.org/10.1111/php.12164>.
- [33] G. Huang, D. Yin, F. Zhang, Q. Li, L. Wang, Yolk@shell or concave cubic NiO-Co₃O₄@C nanocomposites derived from metal-organic frameworks for advanced lithium-ion battery anodes, *Inorg. Chem.* 56 (2017) 9794–9801. <https://doi.org/10.1021/acs.inorgchem.7b01296>.
- [34] F.A. Harraz, R.M. Mohamed, A. Shawky, I.A. Ibrahim, Composition and phase control of Ni/NiO nanoparticles for photocatalytic degradation of EDTA, *J. Alloys Compd.* 508 (2010) 133–140. <https://doi.org/10.1016/j.jallcom.2010.08.027>.
- [35] R.C. Pawar, S. Kang, J.H. Park, J.H. Kim, S. Ahn, C.S. Lee, Evaluation of a multi-dimensional hybrid photocatalyst for enrichment of H₂ evolution and elimination of dye/non-dye pollutants, *Catal. Sci. Technol.* 7 (2017) 2579–2590. <https://doi.org/10.1039/c7cy00466d>.
- [36] J. Xu, Y. Cui, Y. Han, M. Hao, X. Zhang, ZnO-graphene composites with high photocatalytic activities under visible light, *RSC Adv.* 6 (2016) 96778–96784. <https://doi.org/10.1039/C6RA19622E>.
- [37] M. Thomas, G.A. Naikoo, M.U.D. Sheikh, M. Bano, F. Khan, Effective photocatalytic degradation of congo red dye using alginate/carboxymethyl cellulose/TiO₂ nanocomposite hydrogel under direct sunlight irradiation, *J. Photochem. Photobiol. A Chem.* 327 (2016) 33–43.
- [38] U.O. Bhagwata, J.J. Wub, A.M. Asiric, S. Anandan, Sonochemical synthesis of Mg-TiO₂ nanoparticles for persistent congo red dye degradation, *J. Photochem. Photobiol. A Chem.* 346 (2017) 559–569.
- [39] I. Ullah, A. Haider, N. Khalid, S. Ali, S. Ahmed, Y. Khan, N. Ahmed, M. Zubair, Tuning the band gap of TiO₂ by tungsten doping for efficient UV and visible photodegradation of Congo red dye, *Spectrochim. Acta A* 204 (2018) 150–157.
- [40] J.-G. Zhang, W.-J. Gong, Y.-S. Guan, H.-X. Li, D.J. Young, J.-P. Lang, Carboxylate-assisted assembly of zinc and cadmium coordination complexes of 1,3,5-tri-4-pyridyl-1,2-ethylenbenzene: structures and visible-light-induced photocatalytic degradation of congo red in water, *Cryst. Growth Des.* 18 (2018) 6172–6184. <https://doi.org/10.1021/acs.cgd.8b01040>.
- [41] F. Lang, D. Sun, J. Liu, H. Wang, H. Yan, Improved size-tunable synthesis of monodisperse NiO nanoparticles, *Mater. Lett.* 181 (2016) 328–330. <https://doi.org/10.1016/j.matlet.2016.06.056>.
- [42] N.N. MohdZorkipli, N.H. MohdKaus, A.A. Mohamad, Synthesis of NiO Nanoparticles through Sol-gel Method, *Procedia Chem* 19 (2016) 626–631. <https://doi.org/10.1016/j.proche.2016.03.062>.
- [43] V.P. Muhammed Shajudeena, M. Sivakumar, S. Saravana Kumar, Synthesis and characterization of NiO nanoparticles by thermal oxidation of nickel sulfide

- nanoparticles, *Mater. Today* 6 (2016) 2450–2456, <https://doi.org/10.1016/j.matpr.2016.04.161>.
- [44] E.M.M. Ibrahima, L.H. Abdel-Rahman, A.M. Abu-Dief, A. Elshafaie, Samar Kamel Hamdan, A.M. Ahmed, The synthesis of CuO and NiO nanoparticles by facile thermal decomposition of metal-Schiff base complexes and an examination of their electric, thermoelectric and magnetic Properties, *Mater. Res. Bull.* 107 (2018) 492–497, <https://doi.org/10.1016/j.materresbull.2018.08.020>.
- [45] R. Selvakumar, B. Nirosh, S. Vairama, T. Premkumar, S. Govindarajan, Synthesis and crystal structure of $[\text{Ni}(\text{Amgu})_2]\text{X}_2$ – Novel solid-state precursors for NiO nanoparticles, *Inorg. Chim. Acta* 482 (2018) 774–778, <https://doi.org/10.1016/j.ica.2018.07.021>.